SUPPLEMENTARY INFORMATION

Nanoscale hydration in layered manganese oxides

Wei Cheng[1], Jerry Lindholm[2], Michael Holmboe[2], N. Tan Luong[2], Andrey Shchukarev[2], Eugene S. Ilton[3], Khalil Hanna[1], Jean-François Boily[2,*]

1. Univ. Rennes, École Nationale Supérieure de Chimie de Rennes, CNRS, UMR 6226, 11 Allée de Beaulieu, 35708 Rennes, France

2. Department of Chemistry, Umeå University, SE-901 87 Umeå, Sweden

3. Physical Sciences Division, Pacific Northwest National Laboratory, Richland WA 99352, USA

*corresponding author: jean-francois.boily@umu.se +46 73 833 2678

Table of Contents

Birnessite characterization

X-ray Diffraction

X-ray reflections of AcidBir were consistent with those of synthetic birnessite from previous studies (JCPDS No. 80-1098, Fig. S1), indicating turbostratically stacked layers with a d_{001} of ~0.73 nm.(1-3) Those of δ-MnO$_2$ were also similar but of lower intensity, which is consistent with their smaller crystallite sizes (59.2 m^2/g for AcidBir and 204 m^2/g for δ-MnO$_2$).

X-ray Photoelectron Spectroscopy

X-ray photoelectron spectroscopy (Figs. S2-S4, Tables S1) was used to evaluate the atomic composition and Average Oxidation State (AOS) of manganese. We find that the Mn 2p region (Fig. S2a) is typical for MnO$_2$.(4) This region was used to determine the atomic ratio because Mn 3s spectra were acquired at a higher pass energy (40 eV instead of 20 eV for the Mn 2p region) to improve the signal-to-noise ratio. Additionally, the Mn 2p region is preferable to determine O/Mn atomic ratios because the kinetic energy, and therefore the depth of origin, of Mn 2p photoelectrons is comparable to those of the O 1s. Mn 3s photoelectrons have, in contrast, considerably higher kinetic energies.

Using the Mn 2p, O 1s and K 2p regions, we find Mn:O:K atomic ratios of 1.00:1.71:0.17 for δ-MnO$_2$ and 1.00:1.62:0.20 for AcidBir. The dominant O species is the inorganic O of MnO$_2$, alongside organic O. No OH sites could be detected. Correction for organic O at 531.9 eV (Table S1) was obtained by accounting for C-OH line at 286.5 eV (3.83 % in δ-MnO$_2$, 2.36 at. % in AcidBir), and for the COOH line at 288.8 eV (2 $\times$ 2.85 % in δ-MnO$_2$, 2 $\times$ 0.85 at. % in AcidBir). This correction decreased O/Mn ratios to 1.38 for δ-MnO$_2$ and 1.49 for AcidBir. Loss of chemisorbed water in vacuum, and the presence of vacancies could explain these lower values that the stoichiometrically expected value of 2. It could also be that the near surface composition of birnessite surfaces probed by XPS (*i.e.* within the first ~10 nm of the topmost region) have an overall composition similar to Mn$_2$O$_3$.

The Mn 3s region was used to estimate the oxidation state of Mn (Fig. S4). This was achieved by using the method of Ilton *et al* (5) which is a more reliable approach than the traditional use of peak splitting (Fig S3). This analysis shows that δ-MnO$_2$ (58% Mn^{IV}, 36% Mn^{III}, 6% Mn^{II}) is more reduced than AcidBir (72% Mn^{IV}, 25% Mn^{III}, 3% Mn^{II}). We explain the substantial reduction of δ-MnO$_2$ to the

prolonged storing time (>2 months). While the resulting charge imbalance brought by these populations is offset by the intercalation of K^+ in the interlayer region, the nearly equivalent XPS-derived K^+ populations (K/Mn=0.17 in δ-MnO$_2$, K/Mn=0.20 in AcidBir) suggest that oxygen vacancies cannot be neglected. No hydroxyl species could be resolved by XPS.

Temperature-Programmed Desorption

To determine conditions under which birnessite can be fully dehydrated, we performed Temperature Program Desorption in a vacuum (<2.5 Torr) chamber (AABSPEC #2000-A). The chamber (AABSPEC #2000-A) was equipped with CaF_2 windows to collect Fourier Transform Infrared (FTIR) spectra, and connected to a quadrupole mass spectrometer to measure effluent H_2O and CO_2. Experiments were performed by heating dry birnessite powder from 40 to 400 °C under at a rate of 10 °C/min. The sample was pressed on a tungsten mesh (unique wire weaving, 0.002 in. mesh diameter) and then squeezed between two stainless steel plates the slit of a a copper heating shaft in the chamber to ensure thermal contact, and temperature was continuously monitored using a K-type thermocouple

FTIR spectra were collected using a Bruker Vertex 70/V FTIR spectrometer equipped with a DLaTGS detector. The FTIR spectra were collected in the spectral range of 600−4000 cm^{-1} at 4 cm^{-1} resolution with 10 Hz forward/reverse scanning rate. We used the Blackman−Harris three-term apodization function with 16 cm^{-1} phase resolution and the Mertz phase correction algorithm. Each spectrum was obtained from 100 co-added spectra and collected over a 89 s period. Time-resolved ,ass spectra were concomitantly collected using a Pfeiffer Vacuum PrismaPlus instrument at preselected masses (*m/z*) of H_2O and CO_2.
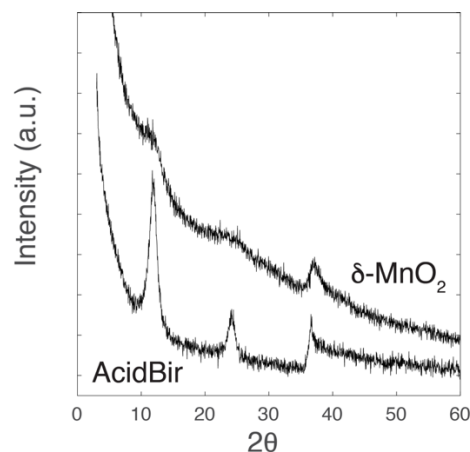
Figure S1. Reflection mode XRD diffractograms from AcidBir (59.2 m^2/g) and δ-MnO$_2$ (204 m^2/g), showing that both phases are birnessite (JCPDS No. 80-1098), with *001, 002, 100* reflections at 2θ=11.99, 24.04 and 36.61°, respectively The small crystallite size of δ-MnO$_2$ is responsible for the low peak intensities, which are nonetheless centered at the same 2θ values.
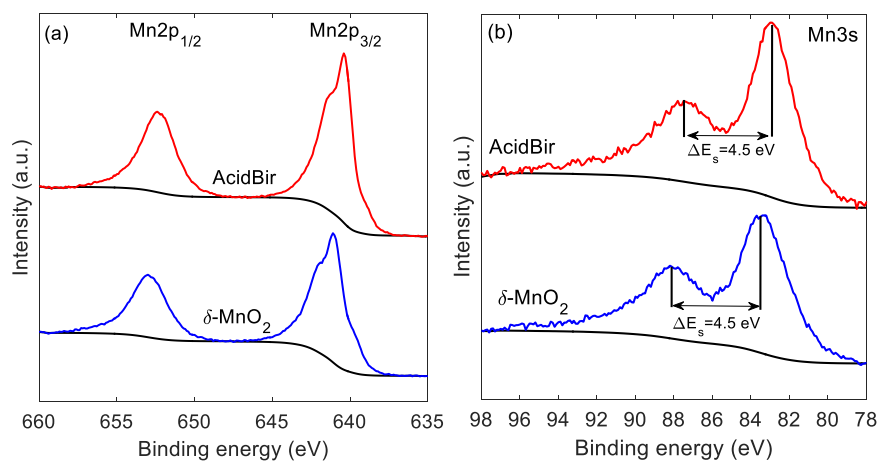

Figure S2. Mn 2p (a) and Mn 3s (b) XPS spectra. Peak splitting of the Mn 3s region is also shown but not used in this work to resolve the average oxidation state of Mn. See Fig. S4 for peak-fitting method used to more confidently evaluate oxidation states.
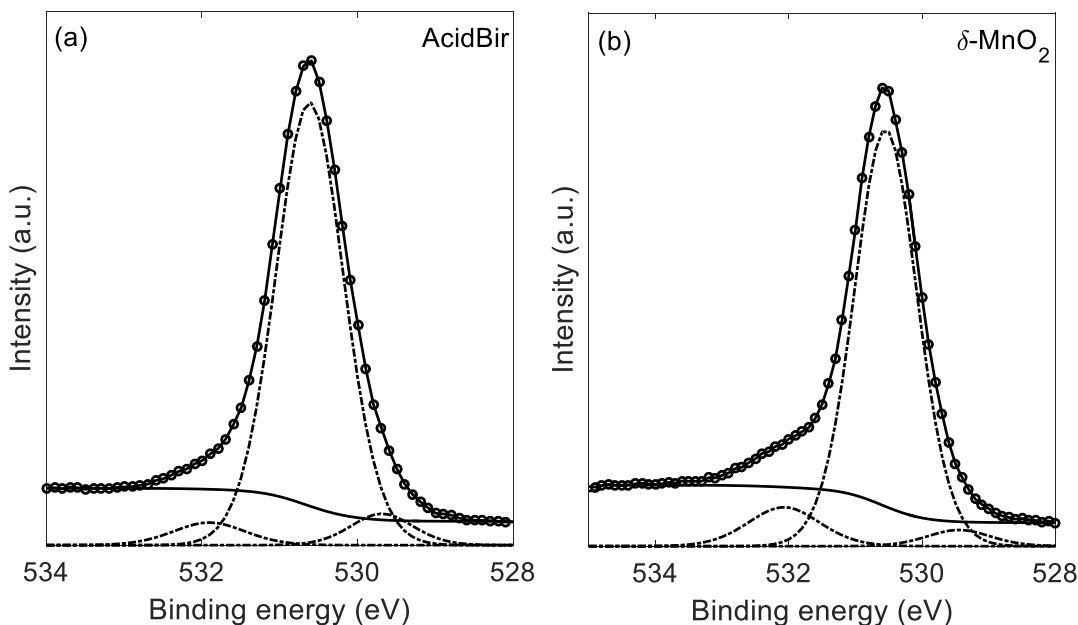
Figure S3. O(1s) spectrum of (a) acid birnessite and (b) δ-MnO₂. The solid curve represents the best fit to the spectral data. The dash-dot curves represent the O component peaks. See Table S1 for peak assignment.
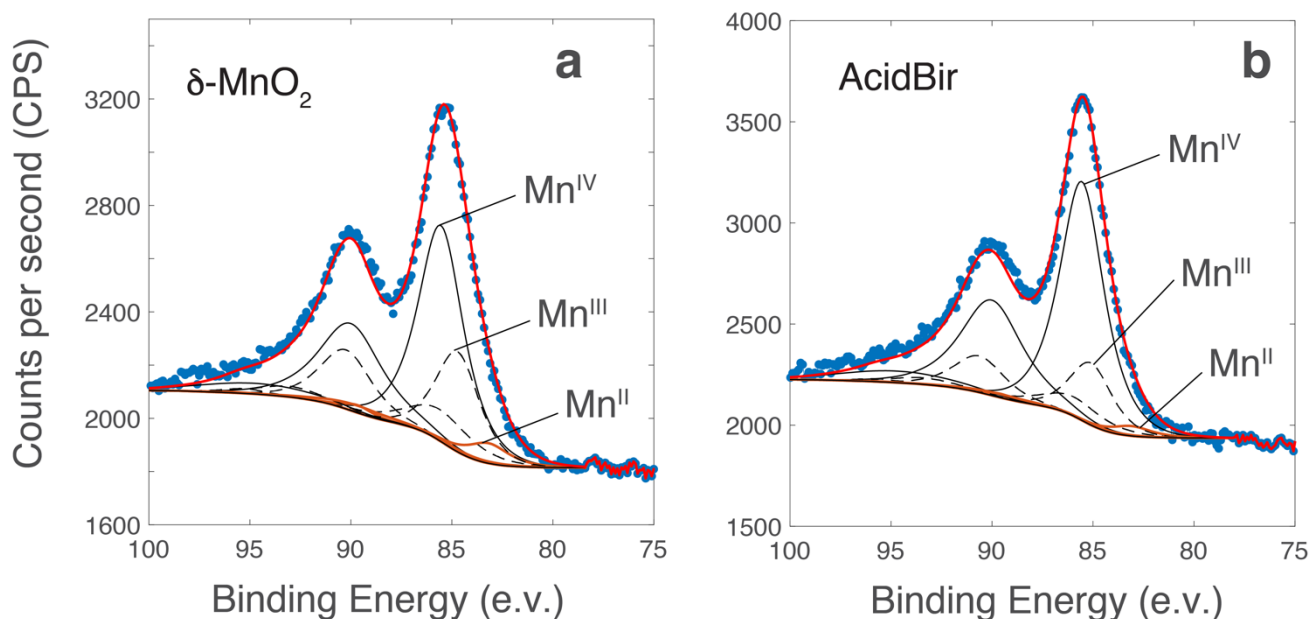

Figure S4. Mn 3s region of (a) δ-MnO₂ and (b) AcidBir fitted with the approach of Ilton *et al. (5)*.

This analysis shows that (a) δ-MnO₂ (58% Mn^{IV}, 36% Mn^{III}, 6% Mn^{II}) is more reduced than (b) AcidBir (72% Mn^{IV}, 25% Mn^{III}, 3% Mn^{II}).
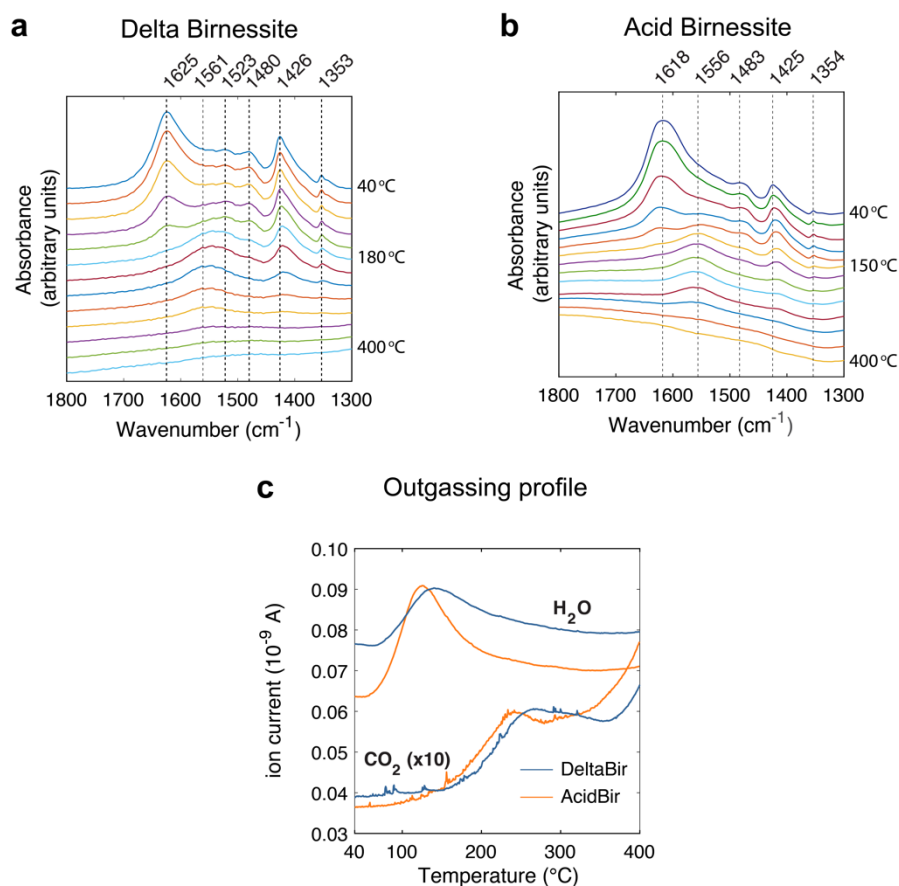
Figure S5. Temperature-Programmed Desorption of water from (a,c) δ-MnO$_2$ and (b,c) AcidBir by transmission FTIR (a,b) and online detection of expelled gases by Quadrupole Mass Spectrometry. The loss of water is confirmed by the water bending (ν_2) mode at 1618-1625 cm^{-1} alongside a dehydration peak at 122 °C for AcidBir and 142 °C for δ-MnO$_2$. Released CO$_2$ arises from adsorbed carbonate species at the birnessite surfaces. Measurements were carried out *in vacuo*.
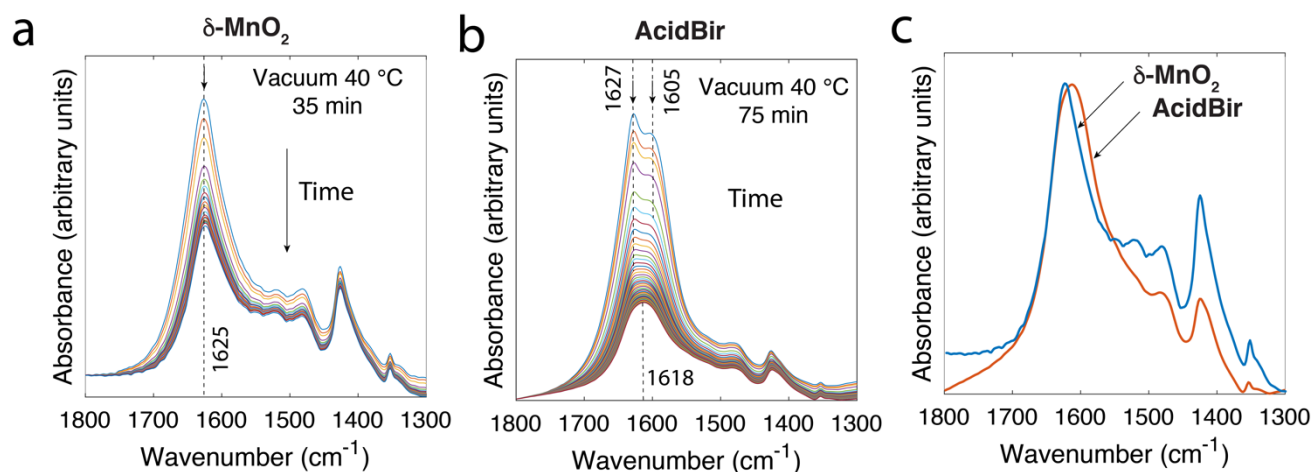

Figure S6. Evacuation of residual water from (a) δ-MnO$_2$ and (b) AcidBir in vacuum (<2.5 mTorr), here monitoring the bending mode (ν_2) of water. Note the double-peak in in AcidBir showing the coexistence of water bound to K$^+$ (1627 cm^{-1}) and associated to vacancies (1605 cm^{-1}). Prolonged evacuation yields resilient populations of water with spectral profiles shown in (c).
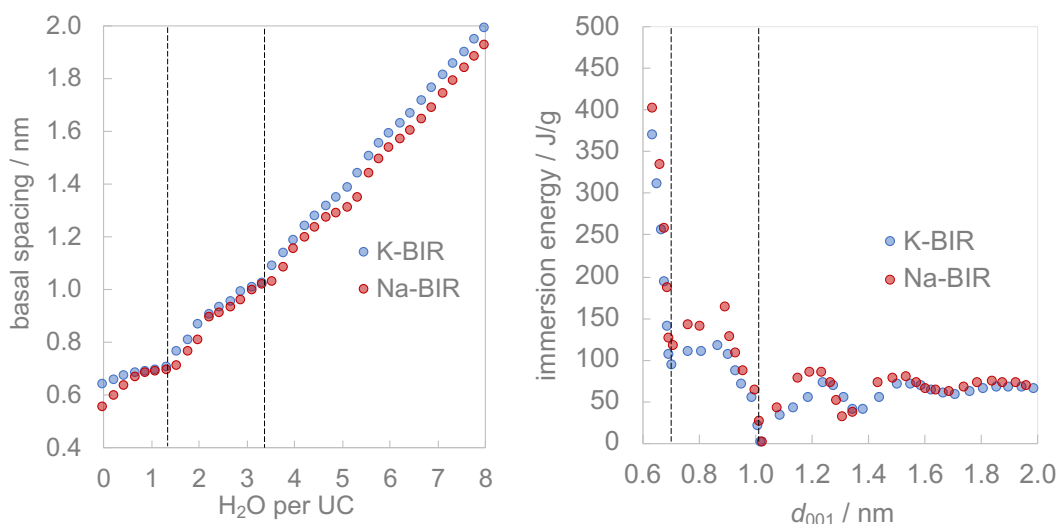
6

Figure S7. Molecular Dynamics simulations of water intercalation in birnessite. (*left*) Basal spacing (d_{001}) data as a function of water molecule populations per unit cell (UC) in K-birnessite (blue) and Na-birnessite (red). (*right*) The corresponding immersion energies as a function of basal spacing. Dashed lines indicate an ideal 1W monolayer (1.33 H_2O/UC, with d_{001}=0.705 nm for K-birnessite; 1.55 H_2O/UC, with d_{001}=0.712 nm for Na-birnessite) and a second theoretical 2W bilayer (3.33 H_2O/UC, with d_{001}=1.02 nm; 3.55 H_2O/UC, with d_{001}=1.03 nm for Na-birnessite) hydration state. These MD results for Na-birnessite align with those of Newton and Kwon (6), who found a slightly smaller maximum water content of 1.42 H_2O/ UC in birnessity of slight larger surface charge (0.29 Na^+/UC).
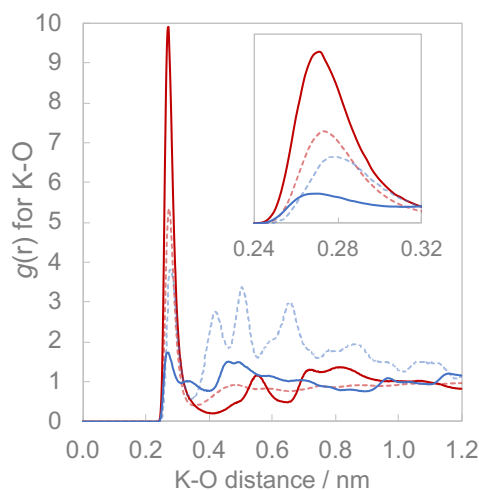

Figure S8. Radial distribution functions, $g(r)$, between K^+ and water (red) and birnessite (blue) oxygen. Solid lines show the ideal 1W state at 0.7 nm, while dashed lines show values at the maximum water loading tested (~13 H_2O/UC).

Table S1. X-ray photoelectron spectroscopy results.

line	δ-MnO$_2$ BE[a]	FWHM[b]	AC (at.%)[c]	AcidBir BE[a]	FWHM[b]	AC (at.%)[c]	Assignment
C 1s	285.0	1.55	10.31	285.0	1.60	4.78	C-(C,H)
	286.5	1.55	3.83	287.2	1.50	2.36	C-O
	288.8	1.60	2.85	289.0	1.00	0.85	COOH
O 1s[d]	529.4	1.10	1.68	529.7	0.95	3.06	Mn=O$_I$
	530.6	1.10	43.02	530.6	1.00	47.32	Mn=O$_{II}$
	531.9	1.25	4.57	531.9	1.05	2.55	Organic O
Mn 2p 3/2	642.2	1.15	28.78	642.9	1.15	32.44	
K 2p 3/2		1.45	4.96	293.2	1.15	6.65	

a. Binding energy (eV), referenced to the C 1s component of aliphatic carbon at 285.0 eV.
b. Full width at half maximum (eV)
c. Atomic concentration in atomic %.
d. A typical value for O in MnO is 529.7 eV and 529.6 for β-MnO$_2$. (4) Surface charging may, however have shifted these components. We find three oxygen species. Mn=O$_I$ and Mn=O$_{II}$ are the two inorganic O species of birnessite.

References

1. Villalobos M, Lanson B, Manceau A, Toner B, & Sposito G (2006) Structural model for the biogenic Mn oxide produced by Pseudomonas putida. *Am. Miner.* 91(4):489-502.
2. Chukhrov FV, Gorshkov AI, Rudnitskaya ES, Beresovskaya VV, & Sivtsov AV (1980) Manganese Minerals in Clays: A Review. *Clays Clay Miner* 28(5):346-354.
3. Manning BA, Fendorf SE, Bostick B, & Suarez DL (2002) Arsenic(III) oxidation and arsenic(V) adsorption reactions on synthetic birnessite. *Environ. Sci. Technol.* 36(5):976-981.
4. Wagner CD (1979) *Handbook of X-ray photoelectron spectroscopy: A Reference Book of Standard Data for Use in X-ray Photoelectron Spectroscopy* (Perkin-Elmer, Cornell University) p 190.
5. Ilton ES, Post JE, Heaney PJ, Ling FT, & Kerisit SN (2016) XPS determination of Mn oxidation states in Mn (hydr)oxides. *Applied Surface Science* 366:475-485.
6. Newton AG & Kwon KD (2018) Molecular simulations of hydrated phyllomanganates. *Geochim. Cosmochim. Acta* 235:208-223.